scientific reports

OPEN

Au L-shell x-ray emission induced by 154.3–423.9 MeV/u C⁶⁺ ions

Xianming Zhou[1,3✉], Jing Wei[1], Rui Cheng[2], Yanning Zhang[1], Yanhong Chen[2], Changhui Liang[1], Xiaoan Zhang[1,2] & Yongtao Zhao[2,3]

The L-shell x-ray emissions of gold are investigated for the bombardment of high energy C⁶⁺ ions in the high energy region of 154.3–423.9 MeV/u. Due to the multiple ionization of outer-shell electrons at the movement of L x-ray emission, the blue shift of the experimental x-ray energy and an enhancement of the relative intensity ratios of Lι, Lβ–Lα x rays are observed. Using the improved thin target formula and considering the effect of multiple ionization on atomic parameters, the L-subshell x-ray production cross sections are extracted from the counts and compared with the theoretical estimations of BEA, PWBA and ECPSSR. It is found that the relative corrections of ECPSSR on PWBA can be ignored in the present experimental energy region. The calculations of PWBA and ECPSSR are almost identical and both are larger than the experimental results. The BEA is in better agreement with the experiment as a whole.

High energy ions have been extensively exploited in different ways in various disciplines, such as, astrophysics, atomic physics, plasma physics, materials physics, biomedicine and so on, for both fundamental research and practical application[1–6]. High energy heavy ions beam is also an alternative driver for the indirect-drive inertial confinement fusion[7–10]. Here, the energy of the driving beam is first converted into x-ray radiation by bombarding of the high energy pulsed beam with a hohlraum made of high-Z material, and then the radiation drives the fuel pellet to implode. Detail knowledge of the conversion efficiency of x-ray radiation and the properties of the radiation field is urgently needed to such indirect drive implosion. In addition, highly charged ions widely exist in the cosmic objects and dense plasma associated with warm-dense-matter and high-energy-density-matter, where they interacts with the surrounding particles to produce x-ray emission, which is affected by the surrounding environment such as the electron temperature, density and other plasma parameters. In turn, the measurement of x-ray emission provides a viable method for the diagnosis of dense plasma[11,12]. Therefore, it is of great significance to further study the x-ray emission induced by high energy heavy ions.

The characteristic x-ray emission, the consequential result from the decay of the projectile ion or inner-shell vacancies produced by collision of energetic ion with atom, provides important information to the arrangement of atomic orbital electron and inner shell process in collisions. In the low and intermediate energy region, a great deal of experimental works have been carried out focusing on such process by x-ray measurement[13–18], and many well-known theories have been developed to describe such inner-shell ionization, such as, binary encounter approximation (BEA)[19], plane wave Born approximation (PWBA)[20], modified PWBA model by energy-loss, Coulomb-repulsion, perturbed-stationary-state and relativistic (ECPSSR) and refined ECPSSR at low energies with modification of united and separated atom approximation (ECUSAR)[21–23]. However, only a limited number of studies have been undertaken in the very high energy region, especially for the fast ions with energy greater than one hundred MeV per mass unit (MeV/u)[24–28]. It is unclear which existing theory molded is more suitable in such a high energy region. Further experiments are required to systematically examine the various simulations.

In energetic ion-atom collisions, the ionization of an inner-shell electron may be accompanied by the ionization of another inner or one or more outer-shell electrons in the same atom. This action, called multi-ionization, is related to the atomic number, charge state, incident energy of projectile and the atomic number of the target atom[29,30]. This can be determined by measuring the blue shift of x-ray energy using a low-resolution semiconductor detector, or analyzing the satellite and hyper-satellite of x-ray spectra with a high-resolution crystal spectrometer. Double K shell ionization produced by fast ions with energies in the tens of MeV/u has been extensively studied by observing the K-shell hyper-satellite lines[31–34]. The multiple ionization induced by low-energy light ions has also been reported by comparing the relative intensity ratio of subshell x-rays[35–37]. It is proposed that the same is anticipated for the bombardment of high energy heavy ions with energies in hundreds of MeV/u.

[1]Ion Beam and Optical Physics Joint Laboratory of Xianyang Normal University and IMP, CAS, Xianyang Normal University, Wenlin Rd. 01, Xianyang 712000, China. [2]Institute of Modern Physics, Chinese Academy of Sciences, Lanzhou 730000, China. [3]School of Science, Xi'an Jiaotong University, Xi'an 710049, China. ✉email: xmzhou19860208@163.com
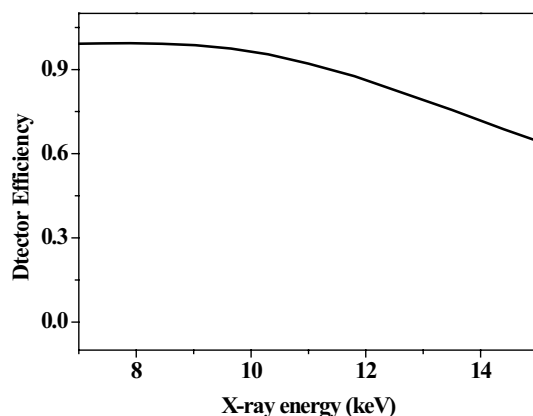
Figure 1. Efficiency of the Silicon Drift Detector.

Therefore, in this work, we would like to present the experimental results of the L-shell x-ray emission of Au produced by the bombardment of high energy C^{6+} ions with energies in hundreds of MeV/u. To confirm the multiple ionization by high energy heavy ions, the energy and the relative intensity ratios of the sub-shell x-ray is obtained and compared with the atomic data. The experimental x-ray production cross sections are calculated and compared with various theoretical simulations to test and verify the applicability of the theory.

Experimental method

The experiment was performed at the cancer therapy terminal at the national laboratory of Heavy Ion Research Facility in Lanzhou (HIRFL) in the Institute of Modern Physics, Chinese Academic of Science (IMP, CAS). The highly charged C^{6+} ions are produced and extracted from the Electron Cyclotron Resonance (ECR) ion source, and then accelerated by the main Cooling Storage Ring (CSRm). The beam quality is improved by a new generation electron cooler, and the corresponding uncertainty of the energies is less than 0.22%. The beam with a duration of 3 ns, and a pulse distance of 15 s was extracted directly into the air and impact perpendicularly on the target after collimation. The beam size measured with a CsI(Tl) crystal is about 5×5 mm, and the beam intensity of impacting on the target is about 10^8 ions/pulse. The initial energies of the accelerated C^{6+} ions in the CSRm are 165, 214, 300, 350 and 430 MeV/u, and the actual energies of the projectile impacting on targets before the collision are about 154.3, 205.0, 292.7, 343.3 and 423.9 MeV/u, respectively, owing to the energy loss passing through the Beryllium window and the air between the target and the exit of the beam line terminal. The number of the incident projectile was measured indirectly by the combined use of a Faraday cup and the counts given by the counter fixed around the exit of the beam line terminal.

The x-rays were observed by a silicon drift detector (SDD) with an effective detection area of 7 mm² and a 12.5 μm Beryllium window in the front of the detector. The SDD was placed 100 mm from the target surface and at a 135 degree angle to the beam direction. The solid angle is about 7×10^{-4} Sr. The detector has an effective energy range of 0.5–14.5 keV when the gain was selected at 100, and an energy resolution of about 136 eV at 5.9 keV when the peaking time is set at 9.6 μs. The energy calibration is performed using simultaneously the two standard radioactive sources of ^{55}Fe and ^{241}Am, and then tested by measuring the K-shell x-rays of Al, V and Fe produced by photon irradiation. In this way, an accurate measurement of the x-ray energy can be guaranteed. The SDD intrinsic efficiency, which combines the transmission effect through the Beryllium window and the interaction in the silicon detector, is determined and provided by the manufacturer of Amptek Company, and is shown in Fig. 1. The target of gold (Au) has a purity of 99.999% with surface area of 15×20 mm² and a thickness of 0.2 mm in the present work.

Results and discussion

1. Au L-shell x-ay spectra induced by C^{6+} ions

Figure 2 shows the typical x-ray emission spectra induced by C^{6+} ions with various incident energies in the range of 154–424 MeV/u. As a comparison, the spectrum by the impact of 300 keV protons is also given, which is measured experimentally on the 1# terminal of the 320 kV high voltage experimental platform at the Institute of Modern Physics, Chinese Academy of Sciences (IMP, CAS) in Lanzhou, China. Due to the absorption of air and the low detection efficiency of the detector in the low energy region, the low energy x-ray spectrum is not recorded in this work. The present spectra are normalized by the number of incident ions (it is about 2.4×10^9 ions) and are well fitted by a nonlinear curve Gaussian fitting program of origin software. For example, the goodness of fit (R-square, R^2) is larger than 0.99. They are regarded as the x rays of Au from the relative decay of L-subshell vacancies.

In Fig. 2, it is obvious that the spectrum consists of four distinct sets of lines, which are identified as Lι, Lα, Lβ and Lγ x ray of Au[38,39]. Lι x ray comes from the radiation transition of M_1 shell electron to L_3 shell vacancy. Lα actually comprise of two x rays which cannot be easily discriminated due to the limitation of the detector,
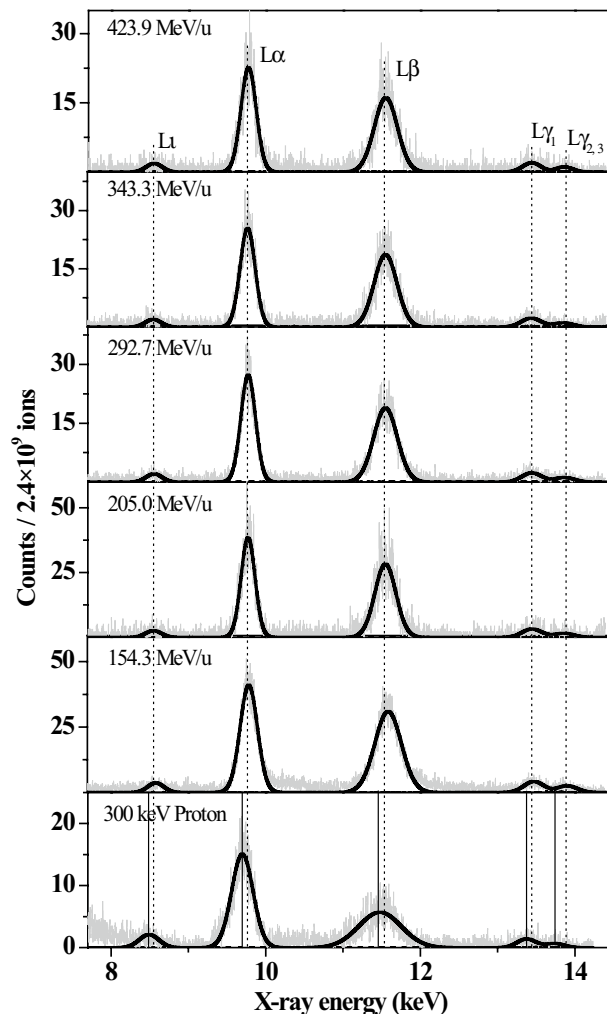
Figure 2. Au L-shell X-ray spectra induced by high energy C^{6+} ions with various incident energy, and compared with that induced by protons.

$L\alpha_1$ and $L\alpha_2$ x ray, and which result from the transitions of M_5-L_3 and M_4-L_3, respectively. $L\beta$ mainly contains six distinguishable spectral lines emitting from the radiation transitions of M_4–L_2, $N_{4,5}$–L_3, M_3–L_1, M_2–L_1, $O_{4,5}$–L_3 and N_1–L_3, which are $L\beta_1$, $L\beta_{2\,15}$, $L\beta_3$, $L\beta_4$, $L\beta_5$, and $L\beta_6$ x ray, respectively. $L\gamma$ is mainly two group lines, $L\gamma_1$ and $L\gamma_{2,3}$ x ray, which are the results of transitions of N_4–L_2 and $N_{3,2}$–L_1, respectively.

One can also find from Fig. 2 that the spectral structures are basically similar for C^{6+} ions with different energies, but they are different from that produced by protons, which can be regarded as a standard spectrum of single ionized atom. Compared to the x-ray emission by protons, the experimental center position of the spectral line induced by the high energy heavy C^{6+} ions is shifted toward the high energy direction. The emission of $L\beta$ x rays are enhanced compared to that of $L\alpha$. That can be interpreted from the influence of multiple ionization of outer-shells on the x-ray emission.

2. Energy shift of the x ray result from multiple ionization

Multiple ionization could be produced in high energy ion-atom collisions or by the impact of lower energy light ions, and can be largely enhanced by heavy-ions bombardment[40–44]. This process causes the formation of multiple vacancies in the outer shells. These vacancies may not be filled before the radiative decay of the inner-shell vacancy, and act as spectators at the moment of inner-shell x-ray emission. This result in a reduction in the screening of nuclear charge and then give rise to increase of the binding energy for all energy levels. As a result, the energy of the x ray emitting from multiply ionized ions is blue shifted.

Table 1 displays the measured energies of Au L-subshell x rays, as well as the results of proton which are almost consistent with the theoretical calculations for single ionized atom and can be regarded as atomic data. The data of high energy C^{6+} ions are all larger than the atomic data, and there is no obvious regular change with the increase of incident energy. Only the result at the incident energy of 154.3 MeV/u is slightly larger than those at other energies. For example, when the energy is 154.3 MeV/u, the blue shifts of $L\iota$, $L\alpha$, $L\beta$, $L\gamma_1$ and $L\gamma_{2,3}$ x ray

	Lι (eV)	Lα (eV)	Lβ (eV)	Lγ$_1$ (eV)	Lγ$_{2,3}$ (eV)
Atomic	8494	9703	11,475	13,379	13,736
Proton	8491 ± 4	9698 ± 3	11,477 ± 5	13,374 ± 4	13,739 ± 5
154.3 MeV/u	8585 ± 5	9786 ± 3	11,588 ± 3	13,472 ± 5	13,902 ± 7
205.0 MeV/u	8549 ± 5	9772 ± 5	11,548 ± 5	13,444 ± 7	13,859 ± 8
292.7 MeV/u	8556 ± 4	9773 ± 3	11,550 ± 4	13,442 ± 5	13,863 ± 6
343.3 MeV/u	8551 ± 3	9771 ± 5	11,554 ± 4	13,437 ± 4	13,852 ± 9
423.9 MeV/u	8549 ± 5	9772 ± 4	11,550 ± 5	13,440 ± 6	13,862 ± 8

Table 1. Au L-subshell x-ray energies induced by high energy C^{6+} ions and 300 keV H^+, and the atomic data [38,39].

	Incident energy of C^{6+} ions (MeV/u)					
	154.3	205.0	292.7	343.3	423.9	Atomic data
Lβ–Lα	0.800 ± 0.112	0.768 ± 0.108	0.777 ± 0.109	0.775 ± 0.109	0.747 ± 0.105	0.580
Lι–Lα	0.079 ± 0.011	0.068 ± 0.010	0.076 ± 0.011	0.075 ± 0.010	0.077 ± 0.011	0.051

Table 2. Relative intensity ratio of Au L-subshell x ray induced by high energy C^{6+} ions.

are 91 ± 5, 83 ± 3, 113 ± 3, 93 ± 5 and 166 ± 7 eV, respectively. However, the average of those shift are 57 ± 4, 69 ± 4, 76 ± 5, 62 ± 6 and 123 ± 8 eV, when the incident energies are at 205.0, 292.7, 343.3 and 423.9 MeV/u, respectively. It is indicated that with the ionization of L-subshell, the M- and N-shell electrons are multiply ionized by the bombardment of high energy C^{6+} ions. In the present experiment, the extent of such multiple ionization is almost constant as a function of the incident energy. This can also be confirmed by the results of the relative intensity ratio of the L-subshell x ray discussed below.

In the approximation of independent-particle framework, multiple ionization can be treated as simultaneous independence single ionization of the orbital electrons, taking electrons correlation effects and subsequent excitation by non-radiation transition out of account[3,29,30,45]. Considering the uniformity of ionization probability of each electron in the same shell, the multi-ionization cross section can be represented by the binomial distribution. The multi-ionization degree is positive to the single ionization cross section[40,45]. The high energy ion-atom collision in the sample can be regard as a binary process, where the inner-shell ionization is mainly determined by the Coulomb interaction between the projectile ions and the electrons in the atomic shell. The cross section of single ionization can be estimated by the BEA model.

According to the calculation of BEA[19], the ionization cross sections of M and N shells of Au in this experiment are on the order of 10^5 and 10^6, respectively, which are 2 and 3 orders of magnitude larger than that of the L shells, respectively, and this cross section decreases with the increase of incident energy. Theoretically, it is expected that the multi-ionization degree of outer-shells is dwindled with increasing incident energy. However, this is not the case. Although, the ionization cross section decreases with increasing incident energy, the extent of such decrease is less than 60%, and it only changes within the same order of magnitude. For instance, the M-shell ionization cross section at the energy of 423.9 MeV/u is only about 40% of that at 154.3 MeV/u. As the incident energy increases from 154.3 MeV/u to 205.0 MeV/u, to 292.7 MeV/u, to 343.3 MeV/u and to 423.9 MeV, the extents of reduction are 35, 15, 12 and 17%, respectively. Therefore, it is proposed that such slow reduction of single ionization cross section does not cause a significant change in the multi-ionization degree in the experiment. This is consistent with the experimental results given in Table 1. To be more specific, the reduced slop of the cross section for the incident energy increasing from 154.3 to 205.0 MeV/u is larger than that in the energy region of 205.0–423.9 MeV/u. When the incident energy is set to 154.3 MeV/u, the cross section of single ionization has a largest value. It is indicated that the multi-ionization degree is at its maximum at the incident energy of 154.3 MeV/u. This is just the reason why the blue shift is the largest at 154.3 MeV/u, as shown in Table 1.

3. Enhancement of the relative intensity ratio of L-subshell x ray caused by multiple ionization

In addition to the blue shift of the x-ray energy, another effect of multiple ionization is to change the atomic parameters. With the presence of multiple vacancies in the outer-shells, some non-radiation transition processes, such as Auger transition and Coster-Kronig, are suppressed due to the absence of multiple electrons in the outer shells. Correspondingly, the probability of radiation transition is enlarged, which leads to the enhancement of the x-ray emission. Such change is related to the single ionization fluorescence yield. As a result, the relative intensity ratio of sub-shell x rays is altered. Table 2 present the experimental relative intensity ratios of Au L-subshell x rays, and that are also shown in Figs. 3 and 4 as a function of incident energy. The experimental data are larger than the theoretical calculations of single ionized atoms, and are almost unchanged with the increase of incident energy. This result indicates that the M and N shells of Au are multiply ionized by the fast C^{6+} ions impact, and such multi-ionization degree is almost independent of the incident energy.
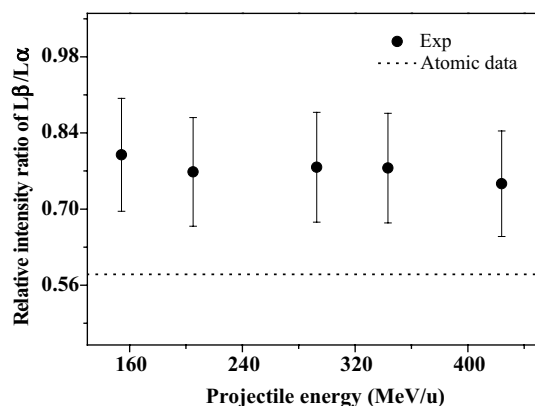
4

Figure 3. Relative intensity ratios of Au Lβ–Lα x-ray induced by C^{6+} ions at different incident energy.
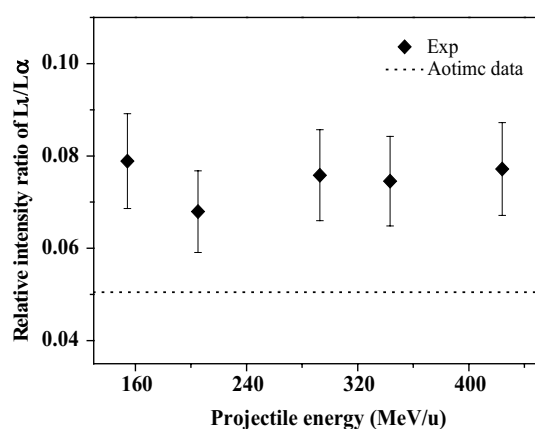

Figure 4. Relative intensity ratios of Au Lι–Lα x-ray induced by C^{6+} ions at different incident energy.

To facilitate discussion, one can divide Lβ x ray into two sets of lines. One is the $L\beta_1$ and $L\beta_{3,4}$ × rays which have a different lower energy level with Lα. The other is $L\beta_{2,15}$, $L\beta_5$ and $L\beta_6$ × rays which have the same lower energy level with Lα. $L\beta_1$ and Lα x rays are mainly the results of the radiation transition of the same upper level $M_{4,5}$ electrons filling the L_2 and L_3 vacancies respectively, and the corresponding fluorescence yields are 0.08 ($\omega_{L\beta1}$) and 0.13 ($\omega_{L\alpha}$) for Au. The Auger yield of L_2 and L_3 sub-shells are 0.544 (a_2) and 0.680 (a_3)[46,47]. These are all in the same scale and there is not much difference. When multiple ionization occurs in the M and N shells, a_2 and a_3 will be reduced by the same amplitude, which will cause the increase of $\omega_{L\beta1}$ and $\omega_{L\alpha}$ to be almost the same magnitude. This will not leads to a significant change in the relative intensity ratio of Lβ and Lα x rays.

However, there is an additional channel for the decay of L_2 vacancies than that of L_3, L_2-L_3X CK transition. Due to the absence of electrons in the outer shells caused by multiple ionization, part of the L_2–L_3X CK process is inhibited, and the fluorescence yield $\omega_{L\beta1}$ is increased. This will result in an enhancement of the $L\beta_1$ x-ray emission. Similarly, the $L\beta_{3,4}$ x-ray emissions, the radiation transition from the decay of L_1 shell, will also be enhanced owing to the outer-shell multiple ionization, because the probabilities of non-radiation transition filling the L_1 vacancies are diminished by the multiple ionization. As a whole result, the relative intensity ratios of $L\beta_{1,3,4}$–$L\alpha_{1,2}$ x-ray increases due to the multiple ionization of M and N shells.

$L\beta_{2,15}$ and Lα x rays are mainly the radiation transitions from the filling of the same lower energy level L_3 vacancies with $N_{4,5}$ and $M_{4,5}$ electrons, respectively. When the M and N shells are multiply ionized, the Auger transition filling the L_3 vacancies is weakened, and the corresponding process of radiation transition is enhanced. The Auger yield a_3 of Au is 1 to 2 orders of magnitude larger than the fluorescence yield of L_3-subshell x ray, which will increase significantly due to the decrease of a_3, and the corresponding x-ray emission will be dramatically enhanced. The fluorescence yield of Lα x ray ($\omega_{L\alpha}$) is about five times as large as that of $L\beta_{2,15}$ ($\omega_{L\beta1,15}$)[46,47]. $\omega_{L\beta2,15}$ is more susceptible to the multiple ionization. Therefore, the increase of $\omega_{L\beta2,15}$ caused by multiple ionization is greater than that of $\omega_{L\alpha}$. This results in a greater enhancement for L $L\beta_{2,15}$ × ray emissions than for Lα x ray. In the same way, the fluorescence yield of $L\beta_5$ ($\omega_{L\beta5}$) and $L\beta_6$ ($\omega_{L\beta6}$) are all about 2 orders of magnitude smaller than $\omega_{L\alpha}$. Under the multiple ionization, the increase of $\omega_{L\beta5}$ and $\omega_{L\beta6}$ is more significant than $\omega_{L\alpha}$. This will cause the increase of the relative intensity ration of $L\beta_{5,6}$ to Lα x ray.

In summary, due to the multiple ionization, the fluorescence yield Lβ x-ray present a larger enhancement than that of Lα. As a result, the Lβ x-ray emission is enhanced than that of Lα, as shown in Fig. 2. And the relative

E (MeV/u)	Lι (10² barn)	Lα (10³ barn)	Lβ (10³ barn)	Lγ (10² barn)	Ltotal (10³ barn)
154.3	2.57 ± 0.44	3.25 ± 0.55	2.60E ± 0.44	5.42E ± 0.62	6.65E ± 1.13
205.0	1.67 ± 0.28	2.46 ± 0.42	1.89E ± 0.32	3.84E ± 0.55	4.91E ± 0.83
292.7	1.38 ± 0.24	1.83 ± 0.31	1.42E ± 0.24	2.87E ± 0.49	3.67E ± 0.62
343.3	1.30 ± 0.22	1.75 ± 0.29	1.36E ± 0.23	2.77E ± 0.47	3.51E ± 0.60
423.9	1.22 ± 0.21	1.59 ± 0.27	1.18E ± 0.20	2.40E ± 0.41	3.13E ± 0.53

Table 3. Au L-subshell x-ray production cross section induced by high energy C^{6+} ions.

intensity ratios of Lβ–Lα x ray are higher than the atomic data, as shown in Fig. 3. But it is no obvious change with increasing incident energy, because the multi-ionization degree is almost a constant with the incident energy.

In the same way, the ratio of I(Lι)/I(Lα$_{1,2}$) can be understood easily. Lι and Lα x rays can be regarded as radiation transitions of different M subshell electrons filling L$_3$ vacancies. The increase of fluorescence yield of those two x ray is only affected by the change in Auger yield a$_3$. The fluorescence yield of Lι x ray ω$_{Lι}$ is much smaller than ω$_{Lα}$, which is only 5%[46,47]. Under the influence of multiple ionization, ω$_{Lι}$ has a greater increase than ω$_{Lα}$. As a result, the emission enhancement of Lι x ray is greater than that of Lα. As shown in Fig. 4, the relative intensity of Lι to Lα x ray is enlarged compared to the atomic data.

4. Au L-subshell x-ray production cross section induced by C^{6+} ions

In the present work, the energy loss of the projectile in the target with an extent of x-ray self-attenuation length does not exceed 0.081 MeV/u, which is much less than the initial incident energy and can be neglected. Therefore, it is proposed that the observed x rays are produced by the swift C^{6+} ions with the same energy, even though they result from the different atomic layers. Taking into account of the self-absorption of the target and the absorption of air between the target and the detector, the experimental x-ray production cross section can be extracted from the thin target formula and can be expressed as[27,48]:

$$\sigma_x = \frac{\sqrt{2}\mu N_x}{\rho N_p \varepsilon_d f_t (\Omega/4\pi)} \cdot \frac{1}{1 - e^{-\sqrt{2}\mu L}} \tag{1}$$

where μ is the absorption coefficient of the x ray. N_X is the obtained counts of the x ray which were extracted by fitting the x-ray spectrum with Gauss function of origin software, namely, the area under peak of the fitted spectral line. ρ is the target atomic number in unit volume. N_p is the number of the incident ions, ε_d is the detector efficiency. f_t is the attenuation factor of the x ray in the air between the target and the detector. Ω is the solid angle. L is the target thickness. The principal errors for the experimental data result from the absorption of air and target 10%, x ray count statistics 5%, incident ions recording 10%, detector efficiency 5% and solid angle 6%, and the maximum error of the total cross section is about 17%.

The experimental results of the L-subshell and total x-ray production cross section are listed in Table 3 as a function of the impact energy of the C^{6+} ions, and are also shown in Fig. 5. This is decreased with increasing impact energy, but the reduction is not large and only changes in the same order of magnitude, while the drop for the energy from 154.3 to 205.0 MeV/u is bigger than that in the energy region of 205.0–423.9 MeV/u. For example, for Lι x ray, the production cross section is about 10^2 barn, which is reduced by about 53% over the entire experimental energy range, while this reduction is about 35% for the energy decreasing from 154.3 to 205.0 MeV, and 18% for 205.0–423.9 MeV. Furthermore, the homologous values for Lα x ray are 10^3 barn, 51, 24, 27% respectively, and 10^3 barn, 55, 28, 27% for Lβ x ray, and 10^2 barn, 56, 30, 26% for Lγ x ray, and 10^3 barn, 53, 26, 27% for the total x ray.

The theoretical L-subshell x-ray production cross section, σ_{Lx}, can be converted from the Li-subshell ionization cross section and is calculated by the following expressions[49,50]:

$$\sigma_{Lι} = \left[\sigma_{L1}\left(f_{13} + f_{12}f_{23}\right) + \sigma_{L2}f_{23} + \sigma_{L3}\right] w_3 F_{3ι} \tag{2}$$

$$\sigma_{Lα} = \left[\sigma_{L1}\left(f_{13} + f_{12}f_{23}\right) + \sigma_{L1}f_{23} + \sigma_{L1}\right] \omega_1 F_{3α} \tag{3}$$

$$\sigma_{Lβ} = \sigma_{L1}\omega_1 F_{1β} + \left(f_{12}\sigma_{L1} + \sigma_{L1}\right)\omega_2 F_{2β} + \left[\sigma_{L1}\left(f_{13} + f_{12}f_{23}\right) + \sigma_{L2}f_{23} + \sigma_{L3}\right]\omega_3 F_{3β} \tag{4}$$

$$\sigma_{Lγ} = \sigma_{L1}\omega_1 F_{1γ} + \left(f_{12}\sigma_{L1} + \sigma_{L2}\right)\omega_2 F_{2γ} \tag{5}$$

$$\sigma_{LTot} = \left[\omega_1 + \omega_2 f_{12} + \omega_3\left(f_{13} + f_{12}f_{23} + f'_{13}\right)\right]s_{L1} + \left(\omega_2 + f_{23}\omega_3\right)\sigma_{L2} + \omega_3\sigma_{L3} \tag{6}$$

where σ_{Li} ($i = 1, 2, 3$) is the ionization cross section of the sub-shell L$_1$, L$_2$ and L$_3$, respectively. f_{ij} is the Coster-Kronig yield for subshells i to j. ω_i is the corresponding i-subshell fluorescence yield. F_{ix} is the fraction of the radiation width of the subshell L$_i$ contained in the x-th spectral line.
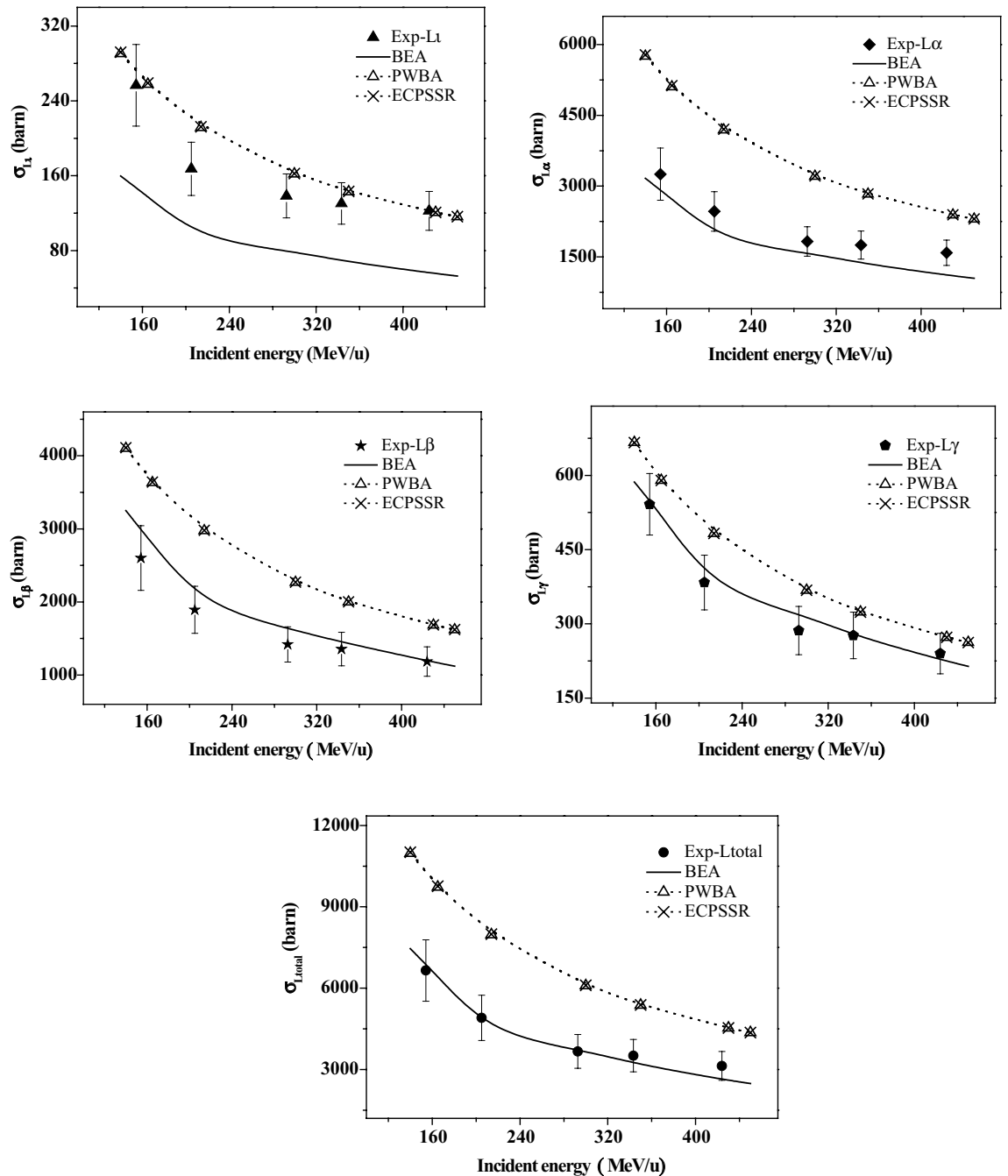
Figure 5. L x-ray production cross section of Au produced by high energy C^{6+}ions, and compared with various theoretical calculations.

As discussed in section 2 and 3 of "Results and discussion", the Au atoms are multiply ionization by the fast C^{6+} ions, which result in the change of x-ray fluorescence yield and probability of no-radiation transition. The theoretical calculation of σ_{Lx} should use the parameters of multi-ionization atom. According to the research by Lapicki et al.[51,52], the multi-ionization fluorescence yield and the CK yield are calculated in the present energy region. In the present calculations, the single ionization atomic values of ω_i and f_{ij} are taken from the work of Campbell[46,47], while the data of F_{ix} is from the tables of Scofield[53,54].

Figure 5 presents the theoretical predictions by the BEA, PWBA and ECPSSR models transformed to the x-ray production cross section, using the multiple ionization atomic parameters. They are all within the same order of magnitude and dwindle with increasing energy. The calculations of BEA are lower than that of PWBA and ECPSSR, which are almost identical, with the largest difference not exceeding 7%. ECPSSR is an improvement over the PWBA. The related corrections are significant in the lower energy region, while this can be neglected in such high energy region in this work.

The experimental-theoretical comparisons are also given in Fig. 5. As a whole, the BEA calculations are in good agreement with the experimental data in spite of the individual small deviation, except for Lι x ray, where

the PWBA and ECPSSR give better estimation of the measured results. For the deviation of Lι, it is proposed that this may be caused by a larger extent anisotropic of Lι emission. In addition, the BEA simulations not only agree basically with the experiment in numerical value, but also present the best prediction of the changing trend, which dwindles faster for the incident energy dropping from 154.3 to 205.0 MeV/u than that from 205.0 to 423.9 MeV/u.

Conclusions

The L-shell x-ray spectra of Au have been measured by bombardment of 154.3–429.3 MeV/u C^{6+} ions. The energy shift and the relative intensity ratio of the L-subshell x rays were investigated as a function of the incident energy, and the experimental x-ray production cross sections were obtained by a well corrected thick target formula and compared with the theoretical estimations of BEA, PWBA and ECPSSR. It is indicated that the Au atom is ionized mainly by direct Coulomb interaction, when it is impinged by high energy C^{6+} ions, which are moving with velocity higher than the orbital velocity of the electrons in the target atom. With the L-shell ionization, the outer-shells are multiply ionized. The multi-ionization degree is considered to be almost constant in the present energy region. This results in a significant blue shift of the x-ray energy and an enhancement of the relative intensity ratios of Lι and Lβ to Lα x ray. It is proposed that the inner-shell ionization of Au should be considered as a binary process between the high energy C^{6+} ions acting as a point charge and the independent target electrons. The L-shell x-ray production cross section can be estimated by the BEA model with the multiple ionization atomic parameters.

Data availability

All data generated or analyzed during this study are included in this published article.

References

1. Xu, G. *et al.* Determination of hydrogen density by swift heavy ions, determination of hydrogen density by swift heavy ions. *Phys. Rev. Lett.* **119**, 207801 (2017).
2. Breuer, L. *et al.* Secondary ion and neutral mass spectrometry with swift heavy ions: Organic molecules. *J. Vac. Sci. Technol. B* **34**, 03H130 (2016).
3. Czarnota, M. *et al.* X-ray study of M-shell ionization of heavy atoms by 8.0–35.2-MeV O^{q+} ions: The role of the multiple-ionization effects. *Phys. Rev. A* **79**, 032710 (2009).
4. Schmelmer, O. *et al.* Particle-induced x-ray emission using high energy ions with respect to microprobe application. *Nucl. Instrum. Methods B* **179**, 469 (2001).
5. Tapper, U. & Räisädnen, J. Comparison of various ions for use in heavy ion induced X-ray emission. *Nucl. Instrum. Methods B* **71**, 214 (2001).
6. Greenberg, J. S., Davis, C. K. & Vincent, P. Evidence for quasimolecular K X-ray emission in heavy-ion collisions from the observation of the X-ray directional anisotropy. *Phys. Rev. Lett.* **30**, 473 (1974).
7. Kawata, S. Direct-drive heavy ion beam inertial confinement fusion: A review, toward our future energy source. *Adv. Phys. X* **6**, 1873860 (2021).
8. Kawata, S., Karino, T. & Ogoyski, A. I. Review of heavy-ion inertial fusion physics, matter and radiation at extremes. *Matter Radiat. Extremes* **1**, 89 (2016).
9. Hofmann, I. Heavy ion accelerator-driven inertial fusion. *Rev. Accl. Sci. Tech.* **08**, 37 (2015).
10. Back, B. B., Esbensen, H., Jiang, C. L. & Rehm, K. E. Recent developments in heavy-ion fusion reactions. *Rev. Mod. Phys.* **86**, 317 (2014).
11. Ciricosta, O. *et al.* Direct measurements of the ionization potential depression in a dense plasma. *Phys. Rev. Lett.* **109**, 065002 (2012).
12. Marshall, F. J. *et al.* Plasma-density determination from X-ray radiography of laser-driven spherical implosions. *Phys. Rev. Lett.* **102**, 185004 (2009).
13. Reyes-Herrera, J. & Miranda, J. K X-ray emission induced by $^{12}C^{4+}$ and $^{16}O^{5+}$ ion impact on selected lanthanoids. *Nucl. Instrum. Methods B* **267**, 1776 (2009).
14. Kahoul, A., Nekkab, M. & Deghfel, B. Empirical K-shell ionization cross-sections of elements from 4Be to 92U by proton impact. *Nucl. Instrum. Methods B* **266**, 4969 (2008).
15. Gorlachev, I. *et al.* X-ray production cross sections induced by neon ions. *Nucl. Instrum. Methods B* **448**, 19 (2019).
16. Lapicki, G. The status of theoretical L-shell x-ray production cross sections by protons based on their revised universal empirical fit. *Nucl. Instrum. Methods B* **467**, 123 (2020).
17. Singh, Y. & Tribedi, L. C. M-subshell x-ray production cross sections of Au induced by highly charged F, C, and Li ions and protons: A large enhancement in the M3 fluorescence yield. *Phys. Rev. A* **66**, 062709 (2002).
18. Cohen, D. D. *et al.* Comparison of proton and helium induced M subshell X-ray production cross sections with the ECUSAR theory. *Nucl. Instrum. Methods B* **318**, 11 (2014).
19. Gryzinski, M. Classical theory of atomic collisions. I. Theory of inelastic collisions. *Phys. Rev. A* **24**, 336 (1965).
20. Johnson, D. E., Basbas, G. & McDaniel, F. D. Nonrelativistic plane-wave Born-approximation calculations of direct Coulomb M-subshell ionization by charged particles. *At. Data Nucl. Data Tables* **24**, 1 (1979).
21. Brandt, W. & Lapicki, G. Energy-loss effect in inner-shell Coulomb ionization by heavy charged particles. *Phys. Rev. A* **23**, 1717 (1981).
22. Lapicki, G. The status of theoretical L-subshell ionization cross sections for protons. *Nucl. Instrum. Methods B* **189**, 8 (2002).
23. Vigilante, M. *et al.* Light-ion-induced Li ionization of 46 ≤ Z ≤ 60 elements: First-and second-order corrections to PWBA. *Nucl. Instrum. Methods B* **51**, 232 (1990).
24. Kondo, C. *et al.* X-ray yields from high-energy heavy ions channeled through a crystal: Their crystal thickness and projectile dependences. *Nucl. Instrum. Methods B* **230**, 85 (2005).
25. Fritzsche, S., Kabachnik, N. M. & Surzhykov, A. Angular distribution of the dielectronic satellite lines from relativistic high-Z ions: Multipole-mixing effects. *Phys. Rev. A* **78**, 032703 (2008).
26. Mei, C. X. *et al.* Zhang X A, K-shell X-ray emission from high energy pulsed C^{6+} ion beam impacting on Ni target. *Acta Phys. Sin.* **66**, 143401 (2017).

27. Zhou, X. M. *et al.* X-ray emission from 424-MeV/u C ions impacting on selected target. *Chin. Phys. B* **25**, 023402 (2016).
28. Zhang, X. A. *et al.* X-ray emission of C6+ pulsed ion beams of CSR impacting on Au target. *Acta Phys. Sin.* **62**, 173401 (2013).
29. Awaya, Y., Kambara, T. & Kanai, Y. Multiple K- and L-shell ionizations of target atoms by collisions with high-energy heavy ions. *Int. J. Mass Spectrom.* **192**, 49 (1999).
30. Hopkins, F., Elliott, D. O., Bhalla, C. P. & Richard, P. Multiple inner-shell ionization of aluminum by high-velocity medium-Z beams. *Phys. Rev. A* **8**, 2952 (1973).
31. Hoszowska, J. *et al.* Physical mechanisms and scaling laws of K-shell double photoionization. *Phys. Rev. Lett.* **102**, 073006 (2009).
32. Horvat, V., Watson, R. L. & Peng, Y. Kα satellite and hypersatellite distributions of Ar excited in heavy-ion collisions. *Phys. Rev. A* **79**, 012708 (2009).
33. Kavčič, M., Kobal, M., Budnar, M., Dousse, J. C. & Tökési, K. Double 1s shell ionization of Si induced in collisions with protons and heavy ions. *Nucl. Instrum. Methods B* **233**, 235 (2005).
34. Kobal, M. Kα and Kβ satellite and hypersatellite fluorescence yields of Mg and Si. *Nucl. Instrum. Methods B* **229**, 165 (2005).
35. Cipolla, S. J. L X-ray intensity ratios for proton impact on selected rare-earth elements. *Nucl. Instrum. Methods B* **261**, 153 (2007).
36. Cipolla, S. J. & Hill, B. P. Relative intensities of L X-rays excited by 75–300 keV proton impact on elements with Z = 39–50. *Nucl. Instrum. Methods B* **241**, 129 (2005).
37. Miranda, J., Lucio, O. G., Téllez, E. B. & Martınez, J. N. Multiple ionization effects on total L-shell X-ray production cross sections by proton impact. *Radiat. Phys. Chem.* **69**, 257 (2004).
38. Deslatters, R. D. *et al.* X-ray transition energies: New approach to a comprehensive evaluation. *Rev. Mod. Phys.* **75**, 35 (2003).
39. X-ray data book: http://xdb.lbl.gov/; Table of Isotopes: http://ie.lbl.gov/atom.htm
40. Czarnota, M. *et al.* Multiple ionization effects in X-Ray emission induced by heavy ions. *Braz. J. Phys.* **36**, 546 (2006).
41. Semaniak, J. *et al.* L-subshell ionization of heavy elements by carbon and nitrogen ions of energy 0.4–1.8 MeV/amu. *Phys. Rev. A* **52**, 1125 (1995).
42. Sarkadi, L. & Mukoyama, T. Measurements of L x-ray production and subshell ionisation cross sections of gold by light- and heavylion bombardment in the energy range 0.4–3–4 MeV. *J. Phys. B Atom. Mol. Phys.* **13**, 2255 (1980).
43. Watson, R. L., Blackadar, J. M. & Horvat, V. Projectile Z dependence of Cu K-shell vacancy production in 10-MeV/amu ion-solid collisions. *Phys. Rev. A* **60**, 2959 (1999).
44. Banaś, D. *et al.* Multiple ionization effects in low-resolution X-ray spectra induced by energetic heavy ions. *Nucl. Instrum. Methods B* **195**, 233 (2002).
45. Kavčič, M., Šmit, Ž & Budnar, M. L-shell ionization in near-central collisions of MeV protons with low-Z atoms. *Phys. Rev. A* **56**, 4675 (1997).
46. Campbell, J. L. Fluorescence yields and Coster-Kronig probabilities for the atomic L subshells. *At. Data Nucl. Data tables* **85**, 291 (2003).
47. Campbell, J. L. Fluorescence yields and Coster-Kronig probabilities for the atomic L subshells. Part II: The L1 subshell revisited. *At. Data Nucl. Data Tables* **95**, 115 (2009).
48. Ouziane, S., Amokrane, A. & Zilabdi, M. Experimental measurements of X-ray production cross-sections by protons of energies between 1 and 2.3 MeV and comparison with theoretical predictions of PWBA and ECPSSR models. *Nucl. Instrum. Methods B* **161–163**, 141 (2000).
49. Kennedy, V. J. *et al.* L X-ray production cross sections and their ratios in Ta, W and Pt for proton impact in the energy range 2–5.2 MeV. *Nucl. Instrum. Methods B* **134**, 165 (1998).
50. Zhou, X. M. *et al.* L x-ray production in ionization of 60Nd by 100–250 keV protons. *Nucl. Instrum. Methods B* **408**, 140 (2017).
51. Lapicki, G. *et al.* Effects of multiple ionization and intrashell coupling in L-subshell ionization by heavy ions. *Phys. Rev. A* **70**, 062718 (2004).
52. Lapicki, G. *et al.* Multiple outer-shell ionization effect in inner-shell x-ray production by light ions. *Phys. Rev. A* **34**, 3813 (1986).
53. Scofield, J. H. Relativistic Hartree-Slater values for K and L X-ray emission rates. *At. Data Nucl. Data Tables* **14**, 121 (1974).
54. Scofield, J. H. Hartree-Fock values of L X-ray emission rates. *At. Data Nucl. Data Tables* **10**, 1507 (1974).

Acknowledgements

Author contributions

X.Z. and Y.Z. conceived the idea and designed the experiment. X.Z., J.W., R.C., Y.C., C.L. and X.Z. carried out the experiment. X.Z. analyzed the data and wrote the manuscript. X.Z., Y.Z. and J.W. reviewed the manuscript. Advices have been given by all the authors.

Competing interests

The authors declare no competing interests.

Additional information

Correspondence and requests for materials should be addressed to X.Z.

Reprints and permissions information is available at www.nature.com/reprints.

Publisher's note Springer Nature remains neutral with regard to jurisdictional claims in published maps and institutional affiliations.